Residue temperatures in intermediate energy nucleus-nucleus collisions

H. M. Xu,[1,2] W. G. Lynch,[1] and P. Danielewicz[1]
[1] *National Superconducting Cyclotron Laboratory and Department of Physics, Michigan State University, East Lansing, Michigan 48824*
[2] *Cyclotron Institute, Texas A&M University, College Station, Texas 77843*
(Received 22 February 1993; revised manuscript received 18 March 1994)

With an improved Boltzmann-Uehling-Uhlenbeck (BUU) model, we have investigated the reaction dynamics leading to the thermal freeze-out for ^{40}Ar+^{124}Sn collisions. Several criteria are assessed for defining the proper thermal freeze-out time which separates preequilibrium processes from equilibrium processes. One of these criteria, the time dependence of the thermal excitation energy, provides consistent results for defining the thermal freeze-out. The other two criteria, the emission rate of nucleons and the quadrapole moment of the momentum distributions, do not consistently provide accurate freeze-out times due to the existence of long time scale collective vibrations. The predicted values for the excitation energies and temperatures, obtained assuming Fermi gas level densities, are quite sensitive to the equation of state and the impact parameter. Surprisingly, both the thermal excitation energies and the residue temperatures, in the limit of a large ensemble of parallel collisions, show little sensitivity to the in-medium nucleon-nucleon cross section.

PACS number(s): 25.70.Pq, 21.65.+f

I. INTRODUCTION

Nucleus-nucleus collisions have proven to be an excellent laboratory for the study of statistical and dynamical features of highly excited nuclear systems [1–5]. These features evolve with incident energy. At incident energies of a few MeV above the Coulomb barrier, the formation of a fully equilibrated compound system (commonly referred to as "complete fusion") and its subsequent statistical decay is the dominant process for central collisions. The statistical decay by emissions of γ-rays, neutrons, and light charged particles as well as fission has been well described by statistical models of compound nuclear decay [6–11]. At incident energies above $E/A \approx$ 15 MeV, however, the situation becomes more complicated. First, complete fusion of projectile and target becomes less likely, and one observes the onset of preequilibrium emission mechanisms [12–21]. Second, the limits of stability and the mechanisms for decay of very hot nuclei are not well understood [22].

Experimental investigations to establish the limits of stability of hot nuclei have frequently focused upon measurements of traditionally well understood residue decay channels which lead to the production of evaporation residues or fission fragments. These measurements indicate that fusionlike processes, particularly for Ar [21–30] or Si [31,32] induced reactions, decrease rapidly with incident energy when $E/A \gtrsim 20$ MeV, and eventually vanish at $E/A \simeq$35–40 MeV, close to the Fermi energy.

Total excitation energies and emission temperatures have also been extracted from the velocities of fusionlike residues [21–30, 33–35] and the spectra of coincident light particle spectra [33–43]. Light particle inclusive spectra have also been analyzed [31,36,37,44–46] to extract temperatures and excitation energies of residues. These analyses suggested that the maximum excitation energy that a nucleus can sustain, decreases with the mass of the composite system, from $E^*/A \approx$ 5–6 MeV for light systems with total masses $A \lesssim 100$, to a value of $E^*/A \approx 3$ MeV for a total mass $A \gtrsim 200$ [33–46].

An alternative study of the thermal and statistical limits of hot nuclei may be obtained by measuring directly the excitation energies and emission temperatures of residues from their decay products. Significant efforts have been made recently, for example, to measure the intrinsic excitation energies of emitted fragments from the relative populations of nuclear states of such fragments [47–73]. These measurements indicate emission temperatures in the range of $T \approx$ 3–6 MeV, which increase gradually with incident energy for incident energies of $E/A \lesssim 200$ MeV. These measurements are also relatively insensitive to the linear momentum transferred to the target residue [60] or the associated multiplicity of charged particles emitted at forward angles [62]. However, there is some evidence that excited state populations are more consistent with thermal models in central collisions than in peripheral collisions [66].

The disappearance of fusionlike cross sections and the observed "limiting" excitation energies and emission temperatures have been frequently interpreted to be a consequence of the instability of hot nuclei at high temperatures [4,5,22–32,74–109]. For example, the static model of Levit and Bonche [82] predict a limiting temperature of $T \simeq$5–10 MeV, above which nuclear matter becomes unstable against hydrodynamic expansion. Calculations of Friedman [74,75] based on nuclear expansion and those of Friedman and Lynch based on surface emission [8] confirm this instability and indicate that hot nuclei undergo a rapid fragment breakup in a narrow window of emission temperature located at about 5 MeV. Dynamical

calculations by Boal *et al.* [103] suggest that constant values of the emission temperature were established quickly over time scales comparable to the time scale for nuclear breakup. Other calculations, using multiparticle phase space models [85–91], or classical molecular dynamics simulations [98,99], suggest that fragmentation can occur at a characteristic temperature whenever hot nuclear systems expand to sufficiently low densities.

In the present paper, we will investigate (1) whether one can reproduce the observed thermal excitation energies and residue temperatures within the Boltzmann-Uehling-Uhlenbeck (BUU) approach; and (2) whether such residual excitation energies and temperatures can carry information concerning the nuclear equation of state and the in-medium nucleon-nucleon cross section. To answer these questions, we have performed improved BUU calculations [110–115]. A brief report of this work was published recently [114]. In Sec. II, the numerical details of the present calculations are described. In Sec. III, the decomposition of the excitation energy and the freeze-out time used in evaluating the residue temperatures are discussed. In Sec. IV, the calculated residue excitation energies and temperatures are investigated as a function of incident energy and impact parameter. The paper is summarized in Sec. V. Some details of the numerical procedures are given in the Appendix.

II. BUU EQUATION IN THE LATTICE HAMILTONIAN APPROXIMATION

A. The BUU equation

We solve the Boltzmann-Uehling-Uhlenbeck equation [116–121]

$$\frac{\partial f_1}{\partial t} + \mathbf{v}\cdot\nabla_r f_1 - \nabla_r U\cdot\nabla_p f_1 = \frac{4}{(2\pi)^3}\int d^3k_2 d\Omega \frac{d\sigma_{nn}}{d\Omega} v_{12}[f_3 f_4(1-f_1)(1-f_2) - f_1 f_2(1-f_3)(1-f_4)], \tag{2.1}$$

where $f = f(\mathbf{r},\mathbf{p},t)$ is the Wigner transformation of the one body density matrix and $\frac{d\sigma_{nn}}{d\Omega}$ and v_{12} are the in-medium cross section and relative velocity for the colliding nucleons, respectively. In Eq. (2.1), U is the total mean-field potential parametrized as

$$U = V_C + U_n + U_{\rm sym}, \tag{2.2}$$

here V_C, U_n, and $U_{\rm sym}$ represent the Coulomb potential, the isoscalar nuclear potential, and the symmetry energy, respectively. In our simulations, the isoscalar mean-field potential U_n (in MeV) is approximated [116,118,119] by

$$U_n = A\rho/\rho_0 + B(\rho/\rho_0)^\gamma, \tag{2.3}$$

where $\rho_0 = 0.17$ fm^{-3} is the saturation value of the nuclear matter density and $\rho = \rho(\mathbf{r})$ is the local density of nuclear matter. Values of $A = -356$ MeV, $B = 303$ MeV, and $\gamma = 7/6$ correspond to a soft nuclear matter equation of state (EOS) with compressibility coefficient $K = 200$ MeV; while $A = -124$ MeV, $B = 70.5$ MeV, and $\gamma = 2$ correspond to a stiff EOS with $K = 375$ MeV. The symmetry potential $U_{\rm sym}$ is represented by

$$U_{\rm sym} = C[(\rho_n - \rho_p)/\rho_0]\tau_z, \tag{2.4}$$

where ρ_n and ρ_p are the neutron and proton matter densities, and τ_z is the isospin operator with eigenvalues $+1$ and -1 for neutrons and protons, respectively. C is a constant with a value $C = 32$ MeV. For simplicity, $\sigma_{NN} = \int d\Omega \frac{d\sigma_{nn}}{d\Omega}$ is chosen to be isotropic and energy independent. The mean-field and the Pauli-blocking factors in the collision integral are averaged over an ensemble of $N_{\rm test}$ parallel simulations, where $N_{\rm test}$ is varied over the range of $50 \le N_{\rm test} \le 300$. Further details of this test particle dependence are discussed in Sec. IV.

B. The lattice Hamiltonian method

The Boltzmann-Uehling-Uhlenbeck equation, given in Eq. (2.1), is most frequently solved by the *test particle* method [116–121], in which the Wigner function f is approximated by

$$f(\mathbf{r},\mathbf{p},t) = \frac{(2\pi\hbar)^3}{N_{\rm test}}\sum_i \delta(\mathbf{r}-\mathbf{r}_i(t))\delta(\mathbf{p}-\mathbf{p}_i(t)). \tag{2.5}$$

Here $N_{\rm test}$ is the number of parallel ensembles and δ is the Dirac delta function. Terms on the l.h.s. of Eq. (2.1) are satisfied by demanding that the test particles follow Newton's equations,

$$\dot{\mathbf{r}}_i = \frac{\partial H}{\partial \mathbf{p}_i} = \frac{\mathbf{p}_i}{m}, \tag{2.6}$$

$$\dot{\mathbf{p}}_i = -\nabla_i U. \tag{2.7}$$

The quality of the numerical algorithm depends on the way the r.h.s. of Eq. (2.7) is evaluated.

In early BUU calculations, the mean field potential U was calculated on a lattice upon which the local density was evaluated by integrating Eq. (2.5) over momentum. The gradient of the mean field potential could be evaluated by taking a difference between the mean field at the neighboring points,

$$(-\nabla_i U)_x = \frac{1}{2l}[U(\rho(k_1-1,k_2,k_3)) - U(\rho(k_1+1,k_2,k_3))]. \tag{2.8}$$

Here l is the lattice spacing, and k_1, k_2, k_3, are the coordinates of the lattice points closest to the particle. An undesirable feature of this algorithm for our purposes is the lack of strict energy conservation. In calculations,

this may be exhibited by spurious emission of nucleons from ground-state nuclei. Over a period of 100 fm/c, the total energy can increase by more than 1 MeV per nucleon [116]. To calculate excitation energies of the order of 2–3 MeV per nucleon, better energy conservation is required.

Lenk and Pandharipande [122] demonstrated that an excellent energy conservation could be obtained if a smooth variation of the force on the test particles in space is imposed, and the force and the nuclear densities on the lattice are calculated consistently. Following these authors, we evaluated the average density ρ_L at lattice location α by smearing out the test particle with a form factor S,

$$\rho_L(\mathbf{r}_\alpha) \equiv \sum_{i=1}^{AN_{\rm test}} S(\mathbf{r}_\alpha - \mathbf{r}_i), \tag{2.9}$$

where $\mathbf{r}_\alpha$ is the position of lattice point α, $\mathbf{r}_i$ the position of particle i, and $N_{\rm test}$ the number of parallel ensembles. The form factor S has the form

$$S(\mathbf{r}) = \frac{1}{N_{\rm test}(nl)^6} g(x)g(y)g(z), \tag{2.10}$$

$$g(q) = (nl - |q|)\Theta(nl - |q|). \tag{2.11}$$

Here, l is the lattice spacing, and $\Theta(x)$ is the step function with values of 1 for $x \geq 0$ and 0 for $x < 0$; n is an integer which determines the range of S. In our calculations, we take $n = 2$ [122]. (The choice, $n = 2$, appears to be required for accurate momentum conservation [122]. It has the consequence that each test particle contributes to the density at 64 different lattice points, leading to rather long computation times for the simulations.) The specific choice of the form factor $S(\mathbf{r})$ in Eq. (2.10) satisfies the normalization condition

$$l^3 \sum_\alpha S(\mathbf{r}_\alpha - \mathbf{r}) = \frac{1}{N_{\rm test}}, \tag{2.12}$$

independent of $\mathbf{r}$, and therefore the total number of particles is exactly conserved:

$$l^3 \sum \rho_L(\mathbf{r}_\alpha) = A. \tag{2.13}$$

It is simple to show that the potential energy density at $\mathbf{r}$ is given by

$$v(\mathbf{r}) = \frac{A\rho_0}{2}\left(\frac{\rho}{\rho_0}\right)^2 + \frac{B\rho_0}{\gamma+1}\left(\frac{\rho}{\rho_0}\right)^{\gamma+1} + \frac{1}{2}\rho_p V_C + \frac{C\rho_0}{2}\left(\frac{\rho_p - \rho_n}{\rho_0}\right)^2, \tag{2.14}$$

where A, B, C, and γ are parameters of the mean field. The total potential energy can be calculated by summing over the lattice points,

$$V = l^3 \sum_\alpha v_\alpha, \tag{2.15}$$

and the total "lattice" Hamiltonian (or total energy) for a classical system of $N_{\rm test}A$ test particles is given by

$$H = \sum_{i=1}^{AN_{\rm test}} \frac{p_i^2}{2m} + N_{\rm test} V. \tag{2.16}$$

With this Hamiltonian, it is straightforward to derive Hamilton's equations of motion for individual test particles:

$$\dot{\mathbf{r}}_i = \frac{\partial H}{\partial \mathbf{p}_i} = \frac{\mathbf{p}_i}{m}, \tag{2.17}$$

$$\dot{\mathbf{p}}_i = -\nabla_i H = -N_{\rm test}\nabla_i V = -N_{\rm test}\sum_\alpha \frac{\partial V}{\partial \rho_\alpha}\nabla_i \rho_\alpha = -N_{\rm test}\sum_\alpha U(\rho_\alpha)\nabla_i \rho_\alpha. \tag{2.18}$$

[Note that for each force calculated by Eq. (2.18), the sum runs over 64 different lattice points, slowing down the simulations significantly.] Since the Hamiltonian is not explicitly time dependent, energy conservation follows because the trajectories of the test particles satisfy Hamilton's equations.

C. Ground state stability and conservation of energy

Figure 1 shows the ground state density distribution determined from Eq. (2.9) for both ^{40}Ar (top) and ^{124}Sn (bottom) nuclei. Both of the computational ground state nuclei have surfaces with an average skin thickness of $r_s \simeq 2.5$ fm (corresponding to the density drop from 90% to 10% of the saturation density) by virtue of the smearing of the test particle density over the lattice. This value of skin thickness is close to the empirical value of $r_{\rm emp} \simeq 2.4$ fm [123].

Figure 2 shows the time dependence of the binding energy per nucleon (top panels), the number of escaped nu-

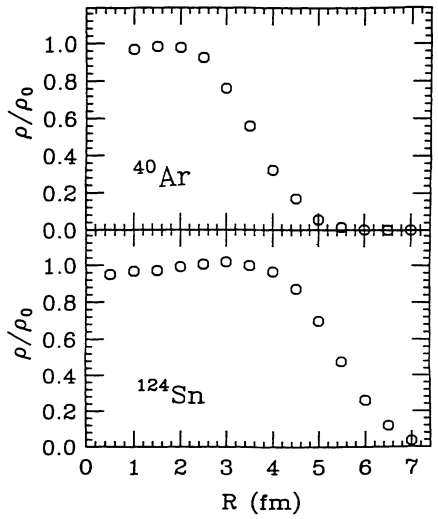

FIG. 1. The density distributions as a function of radius for ^{40}Ar (top window) and ^{124}Sn (bottom window) nuclei.

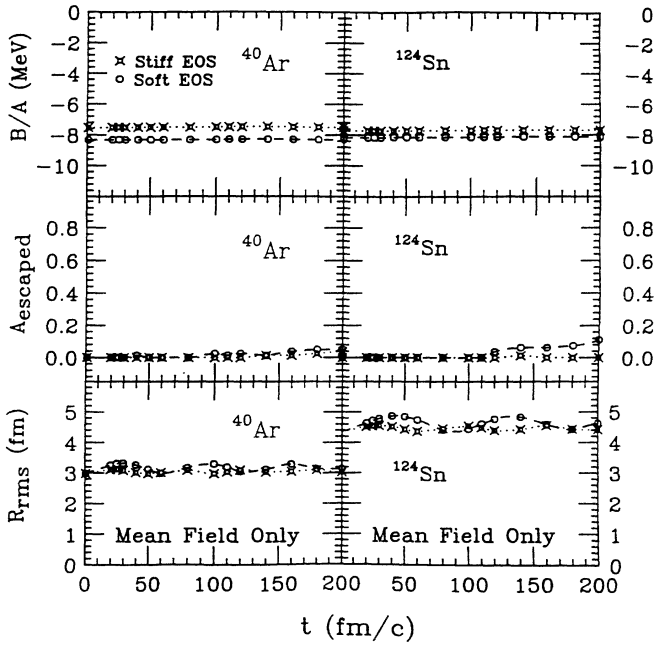

FIG. 2. Stability tests and the conservation of energy for the ground states of ^{40}Ar (left column) and ^{124}Sn (right column) nuclei. The top windows display the binding energy per nucleon predicted by both the soft equation of state (open circles) and the stiff equation of state (open crosses) calculated from Eq. (2.16). The central and bottom windows display, respectively, the number of escaped particles, $A_{\rm escaped}$, and the root-mean-square radius $R_{\rm rms}$ (see the text).

cleons (center), and the rms radius (bottom) for ^{40}Ar (left side) and ^{124}Sn (right) nuclei propagated in the mean field according to the lattice Hamiltonian method. In this figure, calculations using the soft equation of state are designated by open circles and calculations using the stiff equation of state are designated by open crosses. One can see that both equations of state produce an effective binding energy of $-B/A \simeq 8$ MeV. The binding energy obtained for calculations with the soft equation of state is somewhat larger since the corresponding potential is deeper at low densities (nuclear surface). The number of escaped particles $A_{\rm escaped}$ is determined by integrating over all particles at densities $\rho < 0.07\rho_0$. The rms radii, which include all test particles, display some slight collective vibrations that are remnants of the initialization procedure.

In our present model, the position and momentum of each nucleon in a nucleus (both the projectile and the target) are initialized using the standard Monte Carlo procedure [116] which distributes nucleons uniformly in a coordinate sphere and a momentum sphere with the radii determined respectively by the corresponding radius and the Fermi momentum of the nucleus. Since this procedure reflects only the average properties of a nucleus (in both coordinate and momentum spaces) rather than distributing nucleons quantum mechanically, which would *strictly* obey the Pauli exclusion principle, the energy of a groundstate nucleus is slightly higher than that for a truly quantum-mechanical ground state, thus causing the slight vibrations in the rms radii (coordinate space). This effect, nonetheless, is too small to be seen in the momentum space as reflected by the flatness of the binding energy (top panels, Fig. 2).

Once nucleon-nucleon collisions are included, spurious emission of nucleons occurs due to insufficient Pauli blocking at the nuclear surface. With a nucleon-nucleon cross section of $\sigma_{nn} = 41$ mb, the average loss in mass is less than 8% over a period of 160 fm/c. The total energy is, nonetheless, well conserved. In our study, we have investigated the dependence of energy conservation on the time step used in the numerical simulations. We find that change in the total energy is less than 0.1 MeV/A during a time interval of 200 fm/c, provided the time step is less than 0.5 fm/c. We have therefore chosen $\delta t = 0.5$ fm/c in all our calculations.

III. DECOMPOSITION OF ENERGY AND FREEZE-OUT CONDITIONS

A. Decomposition of the excitation energy

Since the residue continues to decay after its formation, the residue masses, excitation energies, and angular momenta are sensitive to the freeze-out time at which observables are evaluated. To indicate how this freeze-out time was chosen and how the thermal energy of the residue was estimated, we decompose the total energy $E_{\rm tot}$ calculated from Eq. (2.16), into collective and internal components, $E_{\rm coll}$ and $E_{\rm int}$, as follows [104]:

$$E_{\rm tot} = H = E_{\rm coll} + E_{\rm int}. \tag{3.1}$$

The collective energy is estimated by

$$E_{\rm coll} = \frac{1}{2} m \int \frac{\mathbf{j}^2(\mathbf{r})}{\rho(\mathbf{r})} d^3r, \tag{3.2}$$

where

$$\rho(\mathbf{r}) = \frac{4}{(2\pi\hbar)^3} \int f(\mathbf{r},\mathbf{p},t) d^3p \tag{3.3}$$

is the local density, and

$$\mathbf{j}(\mathbf{r}) = \frac{4}{(2\pi\hbar)^3} \int \frac{\mathbf{p}}{m} f(\mathbf{r},\mathbf{p},t) d^3p \tag{3.4}$$

is the local collective velocity field. The internal energy $E_{\rm int}$ can be decomposed into a thermal excitation energy $E^*_{\rm the}$ and a "cold" internal energy $E_{\rm int}(T=0, A_{\rm res})$:

$$E_{\rm int} = E^*_{\rm the} + E_{\rm int}(T=0, A_{\rm res}), \tag{3.5}$$

where $A_{\rm res}$ denotes the residue mass. $E_{\rm int}(T=0, A_{\rm res})$ is the internal energy of a cold nucleus with the same density distribution, $\rho(\mathbf{r})$. It includes both the kinetic energy density $\tau(\mathbf{r})$ due to Fermi motion (required by the Pauli exclusion principle) and the potential energy density $v(\mathbf{r})$:

$$E_{\rm int}(T=0,A_{\rm res}) = \int [\tau(\mathbf{r}) + v(\mathbf{r})] d^3r. \qquad (3.6)$$

In the Thomas-Fermi limit, $\tau(\mathbf{r})$ has the form

$$\tau(\mathbf{r}) = \frac{3}{10}(3\pi^2)^{2/3}\frac{\hbar^2}{m}[\rho_p^{5/3}(\mathbf{r}) + \rho_n^{5/3}(\mathbf{r})]. \qquad (3.7)$$

The potential energy density $v(\mathbf{r})$, given by Eq. (2.14), includes both nuclear and Coulomb interactions. From Eqs. (3.1)–(3.7), it is clear that the thermal excitation energy of the residue is obtained, after the collective energy and cold Fermi energy for the zero-point motion are subtracted from the total excitation energy of the residue.

It is instructive to consider the various excitation energy components contained in Eqs. (3.1)–(3.6) for the case of an isolated nucleus at its ground state. Obviously such a nucleus should have no collective energy, $E_{\rm coll} = 0$, and no thermal excitation energy, $E^*_{\rm the} = 0$. The total energy $E_{\rm tot}$ is therefore equal to the internal energy $E_{\rm int}(T = 0, A_{\rm res})$ of a ground-state nucleus with a central density $\rho = \rho_0$. In our later discussions, we denote this energy of ground state by $E_{\rm g.s.}(A_{\rm res})$. Obviously, $E_{\rm g.s.}(A_{\rm res})/A_{\rm res}$ should be about -8 MeV on the average; however, this result is not obtained unless one corrects for spurious collective motion. Because of the finite numbers of test particles at each of the lattice points in the numerical simulations, calculations of the local current $\mathbf{j}(\mathbf{r})$ via Eq. (3.4) yield nonzero values even if the whole nucleus is at rest. This results in a positive value for the collective energy $E_{\rm coll}$, calculated via Eq. (3.2). This spurious collective energy, arising from finite statistics of test particles, can nevertheless be easily estimated, and we provide methods for determining this spurious collective energy in the Appendix. After subtracting this spurious collective energy, the application of Eqs. (3.1)–(3.6) always yields a negligible collective energy for an isolated nucleus in its ground state. Such spurious contributions to the collective energy have been subtracted from all our calculations using the momentum analysis method discussed in the Appendix.

B. Freeze-out conditions

In general, the excitation energies of residues vary continuously with time in our calculations. Nevertheless, in each simulation an unique maximum in the thermal excitation energy following the preequilibrium cascade can be identified. This defines a freeze-out time where the maximum thermal excitation energy of an equilibrated residue is achieved. The sensitivity of this maximum thermal excitation energy to different parameter choices for the BUU transport equation is one of the major focuses of this paper. We further evaluate the appropriateness of this freeze-out criterion by examining the nucleon emission rate and the quadrapole moment of the momentum distribution. Variations of the two latter quantities did not contradict our assignments of the freeze-out time. The sole variation of these two quantities with time, however, did not provide clear signatures for the freeze-out time due to the presence of long time scale macroscopic oscillations.

1. Thermal excitation energy

In Figs. 3 and 4, we display the decomposition of the excitation energy for ^{40}Ar+^{124}Sn collisions at $b = 0$ fm, assuming a soft EOS (Fig. 3) and a stiff EOS (Fig. 4), respectively. Several features of the reaction dynamics are immediately apparent. First, from the time dependence of potential energy (bottom curve), it is clear that the system undergoes a compression during first 30 fm/c, an expansion between 30 fm/$c \lesssim t \lesssim$ 100 fm/c (70 fm/c for the stiff EOS), and finally a relaxation to a more tightly bound configuration at 160 fm/c (120 fm/c for the stiff EOS) for calculations with the soft EOS. The binding energy $E_{\rm int}(T = 0)$ (third curve from the bottom) exhibits a similar behavior at a smaller scale. Second, the energy of free particles increases rapidly after $t \gtrsim 40$ fm/c, suggesting much of the collective energy $E_{\rm coll}$ is taken away by particle emission. Finally, the thermal energy, $E^*_{\rm the}$, which is our particular interest, exhibits two maxima: one global maximum at $t \approx 30$ fm/c and one local maximum at $t_{\rm fre} \approx 160$ fm/c ($t_{\rm fre} \approx 120$ fm/c for stiff EOS). The maximum at $t \approx 30$ fm/c is partly an artifact of the initial momentum distributions, in which the longitudinal velocities of the projectile and the target nuclei cancel each other, causing a minimum in the computation of the collective energy. Because this first maximum occurs during the preequilibrium cascade, it cannot be associated with the maximum thermal excitation energy of an equilibrated residue. The second maximum occurs after the initial preequilibrium stages have finished and

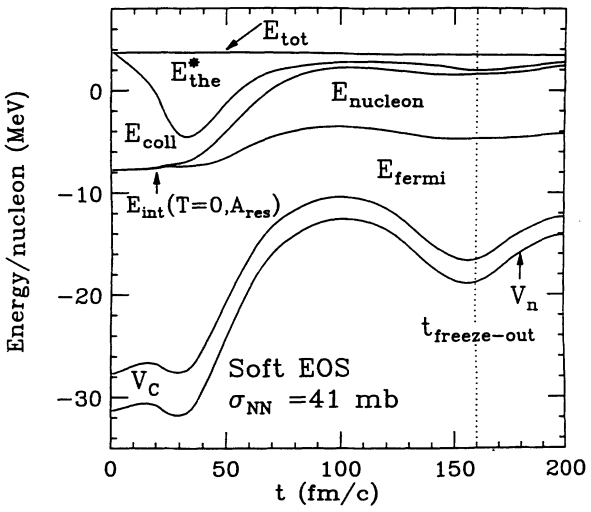

FIG. 3. Decomposition of the excitation energy as a function of time for ^{40}Ar+^{124}Sn collisions with the soft EOS at $E/A = 65$ MeV, $b = 0$ fm. The bottom line is the nuclear potential energy. From this bottom line up are, respectively, Coulomb energy (difference between the second and the bottom lines), Fermi energy required by the Pauli exclusion principle (difference between the third and second lines), kinetic energy of emitted particles (difference between the fourth and third lines), collective energy of bound nucleons (difference between the fifth and fourth lines), and thermal energy (difference between the top and fifth lines). The freeze-out time is indicated by the dotted line.

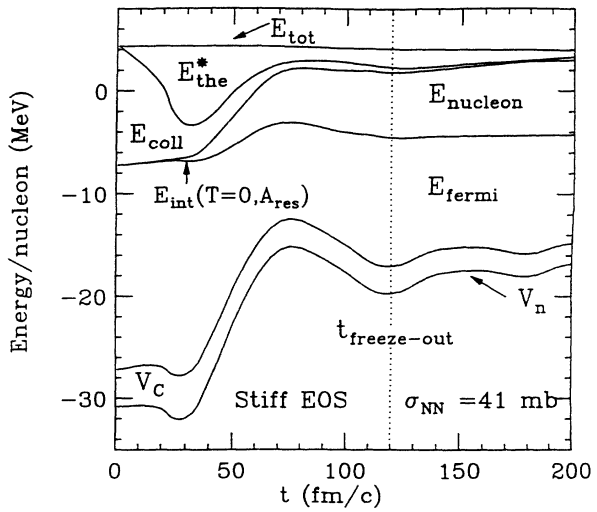

FIG. 4. Same as in Fig. 3 but for ^{40}Ar+^{124}Sn collisions with the stiff EOS at $E/A = 65$ MeV, $b = 0$ fm.

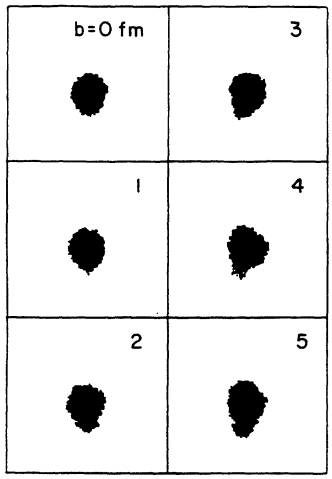

FIG. 5. The spatial distributions at freeze-out for ^{40}Ar+^{124}Sn collisions at $E/A = 35$ MeV with the soft EOS and $\sigma_{NN} = 41$ mb. The values for the impact parameters are indicated in each panel. The beam moves in the vertical direction. (The projectile moves from top to bottom.)

the residue has contracted to a more compact spatial configuration; the thermal energy gradually decreases at later times due to the evaporative cooling. The second maximum in the thermal excitation energy is clearly the maximum thermal excitation energy following the pre-equilibrium cascade; we label the time corresponding to this maximum as the freeze-out time. As shown by the dotted lines in Figs. 3 and 4, the freeze-out times t_{fre} for ^{40}Ar+^{124}Sn collisions are $t_{fre} \approx 160$ fm/c and $t_{fre} \approx 120$ fm/c, respectively, for the soft and stiff EOS at b=0 fm and $E/A = 65$ MeV. Similar analyses lead to $t_{fre} \approx 140$ ($t_{fre} \approx 120$) fm/c at $E/A = 35$ MeV, for the soft (stiff) EOS at $b = 0$ fm.

It is interesting to note that, for these systems, the freeze-out times are largely determined by the relaxation time of the nuclear surface. Residues calculated with the stiff equation of state, which has a larger restoring force and a larger sound speed, contract to compact configurations more rapidly than residues calculated with the soft equation of state. The freeze-out times also depend weakly on the impact parameter at $E/A = 35$ MeV, but more sensitively on the impact parameter at $E/A = 65$ MeV, particularly for the soft EOS. For example, the freeze-out time for ^{40}Ar+^{124}Sn collisions decreases from $t_{fre} \approx 160$ fm/c at $b = 0$ fm to $t_{fre} \approx 120$ fm/c at $b = 6$ fm for the soft EOS and $\sigma_{nn} = 41$ mb. The corresponding freeze-out time for the stiff EOS decreases from $t_{fre} \approx 120$ fm/c at $b = 0$ fm to $t_{fre} \approx 100$ fm/c at $b = 6$ fm.

The final spatial configurations of the bound nuclear matter at freeze-out also depend on the incident energy. At $E/A = 35$ MeV, the freeze-out configurations shown in Fig. 5 reveal a single well defined residue at freeze-out up to impact parameter $b = 6$ fm. The system, at $b = 6$ fm (not shown), subsequently decays into two large slow moving fragments at a *later* time. At $E/A = 65$ MeV, however, the freeze-out configurations, shown in Fig. 6, are more irregular and for $b \gtrsim 2$–3 fm display two or more bound residues at freeze-out. While the thermal excitation energies in this paper were always evaluated for the heaviest residue, these energies change little when all bound fragments are included. The irregular configurations in Figs. 5 and 6 indicate that our freeze-out criterion is achieved well before the collective motion is damped to levels consistent with a thermal equilibrium between collective and intrinsic degrees of freedom. The damping of collective motion would require long time scales consistent with the damping widths of giant resonances. As experimental investigations are sensitive to maximum residue temperatures which are achieved prior to the damping of these giant oscillations, we do not wait for the collective energy in these simulations to be fully thermalized.

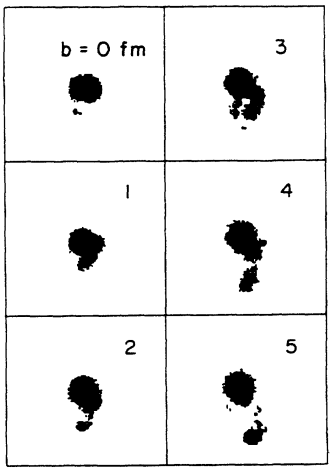

FIG. 6. Same as in Fig. 5 but for collisions at $E/A = 65$ MeV.

2. Emission rate

Nucleons are considered as emitted when their local densities are less than $0.07\rho_0$. Otherwise, they are treated as bound in residues. In Figs. 7 and 8, we display the emission rate of nucleons as a function of time for ^{40}Ar+^{124}Sn collisions at $E/A = 35$ MeV and 65 MeV, respectively. The solid and open circles in the figure depict calculations with the stiff and the soft equations of state, respectively. The corresponding nucleon-nucleon cross sections are indicated in the figures. For all calculations, one observes large preequilibrium emission rates at t $\approx 60 - 80$ fm/c. In contrast, the emission rates at $t \gtrsim 120$ fm/c for stiff EOS, and $t \gtrsim 140$ fm/c for the soft EOS, are significantly reduced and slowly varying, suggesting a slow statistical emission from the reaction residue. These later emission rates are also modulated by macroscopic vibrations which can also be seen clearly in the Q_{zz} plot discussed below. The presence of the modulations renders the establishment of precise freeze-out times from the time dependence of the nucleon emission rate somewhat difficult. The solid and open arrows in Figs. 7 and 8 indicate freeze-out times corresponding to the maxima of the thermal excitation energy discussed in the preceding section. In all cases, these freeze-out times occur shortly after the cessation of the preequilibrium nucleon emission, corresponding to the end of the early preequilibrium stages of the reaction.

3. Momentum distribution

A third measure for defining the freeze-out time may be obtained from the quadrapole moment of the momentum distribution [124]:

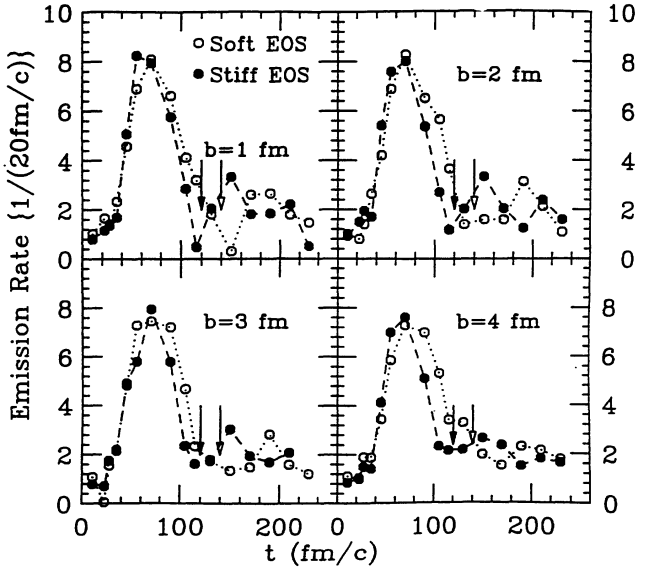

FIG. 7. The emission rates of ^{40}Ar+^{124}Sn collisions at $E/A = 35$ MeV for impact parameters $b = 1 - 4$ fm. The solid circles are results with stiff EOS and the open circles are results with soft EOS. The corresponding freeze-out times are indicated by the arrows (solid for the stiff EOS and open for the soft EOS). The respective lines are used to guide the eyes.

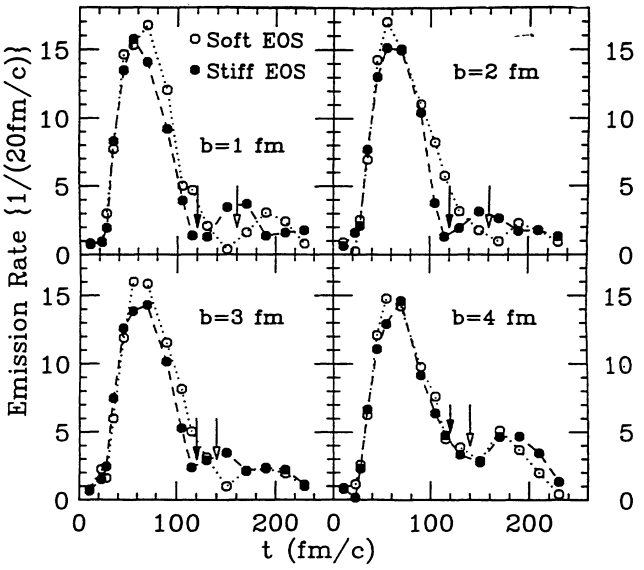

FIG. 8. Same as in Fig. 7, but calculated at $E/A = 65$ MeV.

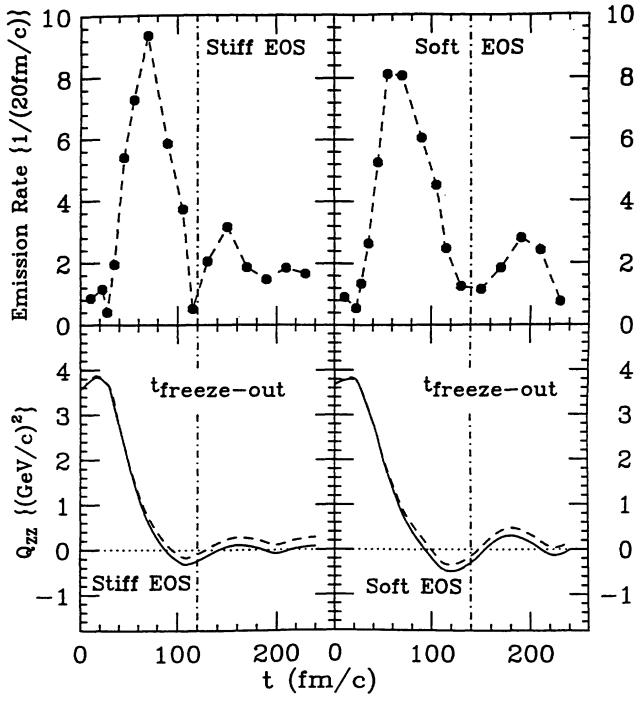

FIG. 9. The emission rates of nucleons (top panels) and the quadrapole momentum distributions Q_{zz} (bottom panels), defined by Eq. (3.8), for ^{40}Ar+^{124}Sn collisions at $E/A = 35$ MeV, $b = 0$ fm. The left panels (right panels) show the results for the stiff EOS (soft EOS). The vertical dot-dash lines indicate the freeze-out time discussed in the text. The dashed lines in the bottom panels include calculations for all nucleons, while the solid lines include only nucleons in the bound residues.

$$Q_{ZZ}(t) = \frac{4}{(2\pi\hbar)^3} \int d^3r d^3p (2p_z^2 - p_x^2 - p_y^2) f(\mathbf{r}, \mathbf{p}, t). \tag{3.8}$$

This criterion is motivated by the belief that an equilibrated system should yield $Q_{ZZ} = 0$. To see how this variable changes with time, we plot Q_{ZZ} in the bottom panels of Figs. 9 and 10 as a function of time for ^{40}Ar+^{124}Sn collisions at $b = 0$ fm. For comparison, we show the emission rates in the top panels. The left panels show results obtained with the stiff equation of state. The right panels show results for the soft equation of state. The dashed lines describe Q_{ZZ} when all nucleons are included, while the solid lines describe Q_{ZZ} when only the nucleons bound in the residual nuclei are included. Clearly at the freeze-out times defined previously, Q_{ZZ} is significantly reduced from its initial value at $t = 0$. However, the values of Q_{ZZ} continue to oscillate about 0 for a long time after thermal freeze-out, reflecting the existence of macroscopic quadrapole vibrations. These long term *collective* vibrations render Q_{ZZ} somewhat less useful in defining the *thermal* freeze-out time. Thus the freezeout defined in the present paper refers to the time at which the preequilibrium is over and the residue becomes nearly completely relaxed and equilibrated.

C. Residue temperature

To allow a comparison with measured residue temperatures, the level densities of the nuclei produced in the simulations must be estimated. These level densities are not trivially related to the total excitation energies of the computational nuclei, because the collective energies of the residues are significant and because the matter densities of the residues are subnuclear. To obtain the required relation between temperature and excitation energy, we approximate the thermal excitation energy of the residue by integrating the Fermi-gas expression $\varepsilon^*(T, \varepsilon_F(\rho(\mathbf{r})))$ for the excitation energy per nucleon over the nuclear density and by equating [114] this value to the thermal energy provided by the numerical simulations,

$$E^*_{\rm the} = \int_C d^3r \{\rho_p \varepsilon^*(T, \varepsilon_F(\rho_p)) + \rho_n \varepsilon^*(T, \varepsilon_F(\rho_n))\}. \tag{3.9}$$

Here, ρ_p and ρ_n are the matter densities for neutrons and protons, respectively. We further approximate $\varepsilon^*(T, \varepsilon_F(\rho))$ by its low temperature limit, and thus Eq. (3.9) becomes

$$E^*_{\rm the} = aT^2, \tag{3.10}$$

with a, the level density parameter, given by

$$a = \frac{m}{3\hbar^2} \left(\frac{3\pi^2}{2}\right)^{1/3} \int_C d^3r \rho^{1/3}(\mathbf{r}). \tag{3.11}$$

In expressions (3.10) and (3.11), we have assumed equal Fermi energies for protons and neutrons, and have used the local density approximation,

$$\varepsilon_F(\rho) = \frac{\hbar^2}{2m} \left(\frac{3\pi^2\rho}{2}\right)^{2/3}. \tag{3.12}$$

In our calculations, the level density parameter is evaluated from the density distribution produced by the BUU calculations at freeze-out. Since our BUU model produces a rather good nuclear surface including its curvature, and since other quantum mechanical effects, such as pairing or shell effects, are washed out in the temperature regime which we are interested, we believe the Fermi-gas formula is a simple and reasonable approximation for addressing questions raised in the present study. In fact, we obtained a value of level density parameter, $a \approx A/8$–$A/9$, comparable to empirical values. Our results are discussed in the following section.

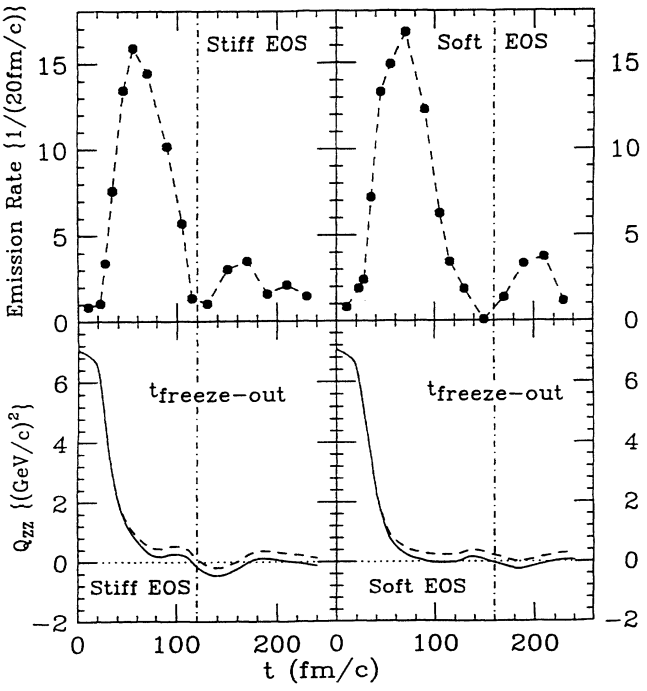

FIG. 10. Same as in Fig. 9, but calculated for ^{40}Ar+^{124}Sn collisions at $E/A = 65$ MeV, $b = 0$ fm.

IV. RESULTS

Partly due to the demands of the lattice Hamiltonian approach, calculations with the present code require very significant amounts of computer time, particularly when the number of test particles is large. In the following sections, we first discuss the sensitivities of the thermal excitation energy and residue temperature to the number of test particles. Then, to explore the qualitative dependences of the residue temperatures upon impact parameter, we have performed some calculations with reduced number of test particles, $N_{\rm test} = 80$. For quantitative comparisons with experimental residue tem-

peratures, however, the incident energy dependences of residue temperatures were calculated with $N_{\rm test}$ =300. In all calculations, the uncertainties in the calculated thermal excitation energies due to test particle statistics were obtained by repeating each calculation many times and examining the variations in the excitation energies which result from variations in the initial random number seeds and in the initial positions and momenta of test particles within the initial projectile and target nuclei.

A. Dependence on the number of test particles

Figure 11 shows the sensitivity of the predicted residue excitation energies (top panels) and temperatures (bottom panels) to $N_{\rm test}$, the number of parallel ensembles, over the range $50 \leq N_{\rm test} \leq 300$, for ^{40}Ar+^{124}Sn collisions at E/A = 35 (right panels) and 65 (left panels) MeV. (Larger values of $N_{\rm test}$ are unfeasible with the present code due to the large computation times required.) Both the thermal excitation energies and residue temperatures increase with $N_{\rm test}$, an effect which may be related to improvements in the accuracy of the Pauli blocking with increasing $N_{\rm test}$. This sensitivity to $N_{\rm test}$ becomes very small for $N_{\rm test} \gtrsim 200$. Significantly larger values of the thermal excitation energies and residue temperatures are obtained for calculations with the stiff EOS, regardless of the value of $N_{\rm test}$. The sensitivity to σ_{NN} decreases with $N_{\rm test}$ and appears to be nearly negligible at $N_{\rm test}$ = 300, possibly reflecting a decrease in the collision rate due to an improved accuracy of the Pauli-type blocking algorithm. For this reason, we concentrate, in the following section, on the sensitivity of the calculations to the EOS. We return later, in Sec. IV C, to the sensitivity to σ_{NN}.

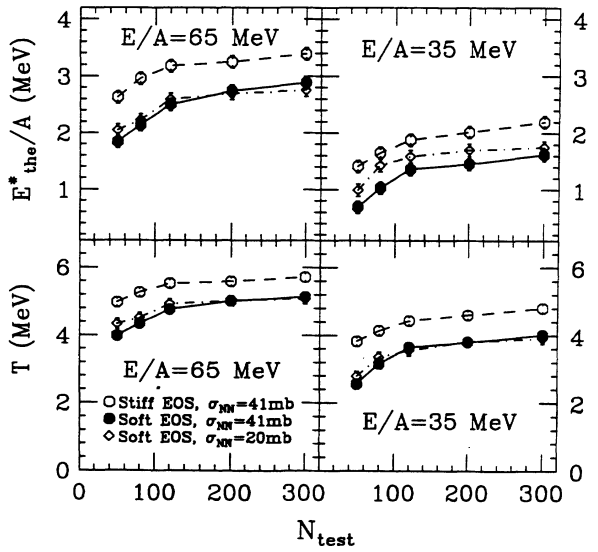

FIG. 11. Dependence of the residue thermal excitation energies and temperatures at thermal freezeout upon the number of parallel ensembles, $N_{\rm test}$, for ^{40}Ar+^{124}Sn collisions at b = 1 fm and E/A = 35 (right panels) and 65 (left) MeV, respectively. The different symbols correspond to calculations with different values of EOS and σ_{NN} indicated in the figure. Details are discussed in the text.

B. Impact parameter dependence

The left side of Fig. 12 shows the predicted thermal excitation energy per nucleon at thermal freeze-out, for $N_{\rm test}$ = 80, as a function of the impact parameter for residues formed in ^{40}Ar+^{124}Sn collisions at E/A = 35 MeV (top window) and E/A = 65 MeV (bottom window), respectively. The uncertainties in the calculated thermal excitation energies are the combination, in quadrature, of the systematic uncertainty in the thermal excitation energy due to the uncertainty in the freeze-out time, and of the random uncertainty due to test particle statistics. For both the stiff and the soft equations of state, these thermal excitation energies were calculated with $\sigma_{NN} = \int \frac{d\sigma_{nn}}{d\Omega} d\Omega$ =41 mb. The observed dependence upon the equation of state partly reflects the fact that preequilibrium emission is enhanced in calculations with the soft EOS for the following reasons. First, the stiff EOS has a larger surface restoring force, and systems simulated with the stiff EOS remain closer to normal nuclear matter density and emit fewer preequilibrium test particles. Second, the stiff EOS also has a larger sound velocity, leading to an earlier thermal freeze-out and consequently less time for cooling via preequilibrium emission. At the higher incident energy where the target nucleus is less effective in capturing nucleons from the projectile, the thermal excitation energies also depend more strongly upon impact parameter than at lower energy.

The right-hand side of Fig. 12 shows the corresponding predictions for the temperatures as a function of impact

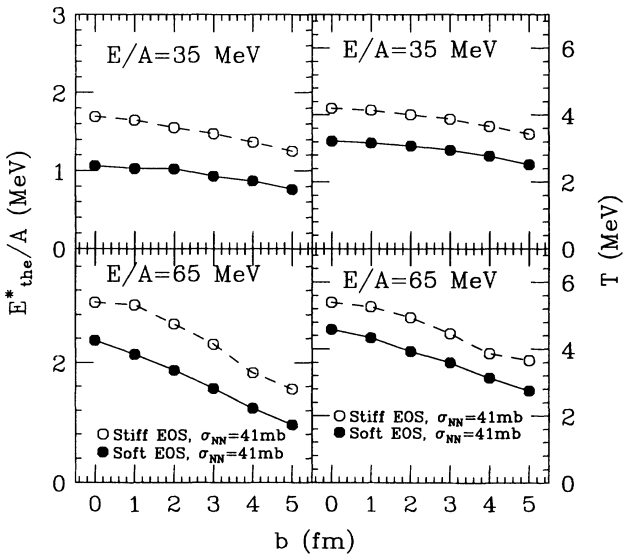

FIG. 12. Sensitivities of the residue thermal excitation energies (left panels) and temperatures (right panels) to the impact parameter and the EOS for ^{40}Ar+^{124}Sn collisions at E/A = 35 MeV (top panels) and 65 MeV (bottom panels), respectively. Details are discussed in the text.

parameter for ^{40}Ar+^{124}Sn collisions at E/A = 35 MeV (top window) and E/A = 65 MeV (bottom window), respectively. At E/A = 35 MeV, the predicted temperature depends weakly on impact parameter, but depends sensitively on the nuclear equation of state. In contrast, the temperature depends rather strongly upon both the impact parameter and the equation of state at higher energies, E/A = 65 MeV. At both incident energies, the higher residue temperatures for calculations with the stiff EOS is partly due to the higher matter density and consequently higher nuclear level density of residues formed in collisions using the stiff EOS, as well as due to the higher residue thermal excitation energies.

C. Incident energy dependence

In Fig. 13, we show the energy dependences of the total excitation energy [111,112] (upper window) and thermal excitation energy (lower window) for ^{40}Ar +^{124}Sn collisions at b = 1 fm. (These calculations were performed with $N_{\rm test}$ =300.) The corresponding residue masses are shown in Fig. 14. In general, calculations with the stiff EOS produce more massive targetlike residues. The masses of these residues decrease roughly linearly with incident energy. For both the stiff EOS (open circles) and the soft EOS (solid circles), the excitation energy per nucleon increases with incident energy. However, this increase with energy becomes more gradual at energies $E/A \gtrsim$ 65 MeV, indicating that the excitation energy per nucleon may be approaching a saturation value. The

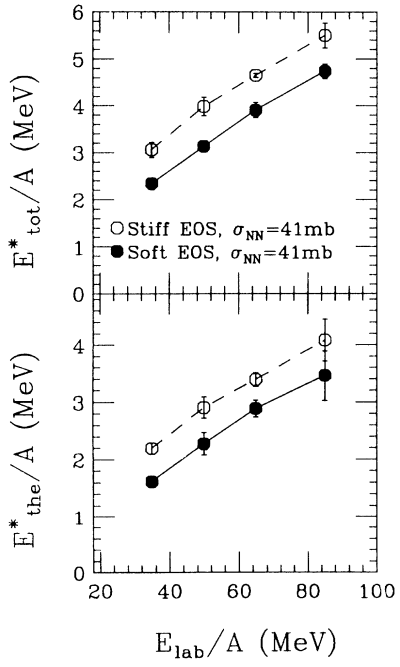

FIG. 13. The dependence of total excitation energy per nucleon (top window), and the thermal excitation energy per nucleon (bottom window) on the incident energy for ^{40}Ar+^{124}Sn collisions at b = 1 fm. The dashed lines represent calculations using σ_{NN}=41 mb and the stiff EOS. The solid lines represent calculations using σ_{NN}=41 mb and the soft EOS.

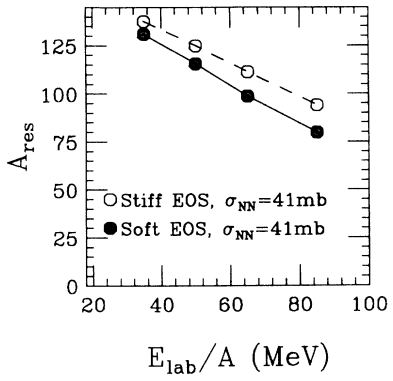

FIG. 14. The dependence of residual mass on the incident energy for ^{40}Ar+^{124}Sn collisions at b = 1 fm.

difference between excitation energies per nucleon for different equations of state is about $\approx$ 1 MeV at all energies.

A saturation has been reported in the total excitation energies deduced from measurements of the multiplicities of neutrons and α particles [33,44]. Since preequilibrium emission carries away more nucleons in our calculations than assumed in the analyses of the neutron and α particle multiplicities [33,44], we do not know whether our calculated total excitation energies are truly comparable to the ones extracted from the experimental data, and therefore, we refrain from making this comparison.

Figure 15 shows the energy dependence of the temperature for the ^{40}Ar+^{124}Sn system at b =1 fm. The dashed lines represent calculations using σ_{NN}=41 mb

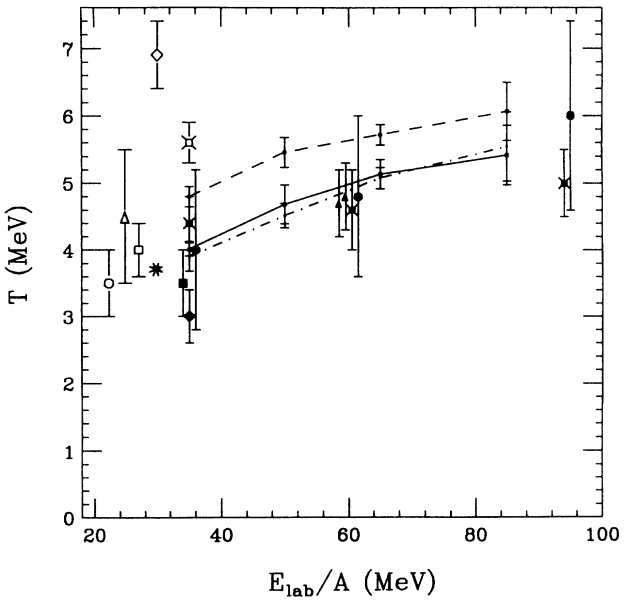

FIG. 15. The dependence of residue temperature on the incident energy for ^{40}Ar+^{124}Sn collisions at b = 1 fm. The dashed lines represent calculations using σ_{NN}=41 mb and the stiff EOS, the solid lines represent calculations using σ_{NN}=41 mb and the soft EOS, and the dash-dotted lines represent calculations using σ_{NN}=20 mb and the soft EOS. The other symbols are experimental data discussed in the text.

and the stiff EOS, the solid lines represent calculations using σ_{NN}=41 mb and the soft EOS, and the dash-dotted lines represent calculations using σ_{NN}=20 mb and the soft EOS. Both equations of state predict a gradual increase in temperature as the incident energy is raised from E/A = 30 MeV to 85 MeV. At higher incident energies, $E/A \gtrsim 50$ MeV, however, the temperature increases very gradually, giving the appearance that the temperature may be approaching a limiting value with incident energy. The stiff EOS predicts consistently larger values of temperature at all incident energies; the calculated residue temperatures are much more sensitive to the variations in the EOS than to the variations in the nucleon-nucleon cross section.

Limiting temperatures have also been deduced from the energy spectra of light particles and from the relative populations of excited states of emitted complex fragments. The data points in Fig. 15 are the experimental temperatures extracted from energy spectra of light charged particles in Refs. [43] (open diamond), [38] (open cross), [41] (solid triangles), [34] (open square), and [46] (open triangle); neutron energy spectra in Ref. [42] (star), and the emission temperatures extracted from excited states in Refs. [60] (solid circles and crosses), [51] (open circle), [69] (solid diamond), and [65] (solid square). Calculations with the soft EOS appear closer to the experimental data. However, due to the strong impact parameter dependences of the calculated residue temperatures, which is not addressed by many of the measurements, we cannot make quantitative conclusions concerning the stiffness of the EOS from the present comparisons. Further alterations in the calculated temperatures may result from additional increases in the number of parallel ensembles, or by allowing for a velocity dependence of the mean field or a different surface behavior.

V. SUMMARY AND CONCLUSIONS

In summary, we have calculated residue excitation energies and temperatures by solving the BUU equation using a lattice Hamiltonian method proposed originally by Lenk and Pandharipande. This method provides accurate energy conservation in practice. Correcting for the spurious collective motion due to finite test particle statistics, we have calculated the maximum thermal excitation energy of targetlike residues following the preequilibrium cascade. To determine the freeze-out time at which this occurs, we have examined the time dependence of the thermal excitation energy. We have identified a maximum shortly after the conclusion of the preequilibrium cascade as the maximum thermal excitation energy of the targetlike residue. Two other variables, the emission rate of nucleons and the quadrapole moment of momentum tensor are consistent with this definition of the maximum thermal excitation energy, but do not provide accurate independent information because of the existence of long time scale collective vibrations. These other two variables may provide more stringent information in more mass asymmetric colliding systems where collective motion may be less strongly excited.

Both the excitation energies and residue temperatures, obtained assuming Fermi gas level densities, are quite sensitive to the equation of state and the impact parameter. Surprisingly, both showed little sensitivity to the in-medium nucleon-nucleon cross section in collisions with large numbers of test particles. The predicted residue temperatures at b = 1 fm for the soft EOS are more comparable with those obtained from experiments than are those obtained for the stiff EOS. However, due to strong impact parameter dependence in the calculations (and presumably in the measured quantities), we cannot make quantitative conclusions concerning the stiffness of the EOS from the present comparisons. Moreover, the present predictions could be altered by using larger numbers of test particles or by allowing a velocity dependence or a different surface behavior for the nuclear mean field.

ACKNOWLEDGMENTS

The authors would like to acknowledge many helpful and fruitful discussions with C.K. Gelbke, M.B. Tsang, and M. Tohyama. W.G.L. acknowledges financial support from the National Science Foundation's Presidential Young Investigator program. This work was supported in part by the National Science Foundation under Grant Nos. PHY-86-11210, PHY-87-14432, and PHY-89-05933, and by the Department of Energy under Grant No. DE-FG05-86ER40256 and by the Robert A. Welch Foundation.

APPENDIX: CORRECTION TO THE COLLECTIVE EXCITATION ENERGY DUE TO FINITE TEST PARTICLE STATISTICS

In our calculations, the collective excitation energy is obtained via Eq. (3.2) which sums up contributions from individual lattice cells wherein the collective current is evaluated using Eq. (3.4). Consider one such lattice cell with K test particles. Suppose this cell has a true collective momentum of $\mathbf{p}_{\rm coll}$ per nucleon in the continuum limit (an infinite number of test particles). The true collective excitation energy of K test particles can be represented by

$$E^0_{\rm coll} = \frac{K p^2_{\rm coll}}{2m}. \tag{A1}$$

Here m is the nucleon mass. In practice, this true collective energy is not known. Instead, we calculate the apparent collective energy $E^a_{\rm coll}$

$$E^a_{\rm coll} = \left\langle \frac{(\sum_i^K \mathbf{p}_i)^2}{2Km} \right\rangle. \tag{A2}$$

Rewriting $\mathbf{p}_i = \mathbf{p}_i{}' + \mathbf{p}_{\rm coll}$ (where $\mathbf{p}_i{}'$ is a random momentum component due to Fermi or thermal motion which vanishes on average),

$$E^a_{\rm coll} = \frac{\left\langle [\sum_i^K (\mathbf{p}_i{}' + \mathbf{p}_{\rm coll})]^2 \right\rangle}{2Km} = \frac{1}{2Km}\left[K^2 p^2_{\rm coll} + \left(\sum_{i=1}^K \mathbf{p}_{\rm coll}\right)\left\langle \sum_{i=1}^K \mathbf{p}_i{}' \right\rangle + \left\langle \left(\sum_{i=1}^K \mathbf{p}_i{}'\right)^2 \right\rangle \right]. \tag{A3}$$

In our simulations, the contributions from the second term can be ignored, since the vector sum will average to zero when one sums over all possible ensembles or over all lattice points. The third term, however, is non-zero and has the approximate value [125]

$$\left\langle \left(\sum_{i=1}^{K} \mathbf{p}_i{}' \right)^2 \right\rangle = K \langle p'^2 \rangle, \tag{A4}$$

where $\langle p'^2 \rangle$ is the average value of the random momentum component due to Fermi or/and thermal motion. Using this expression, Eq. (A3) becomes

$$\begin{aligned} E^a_{\rm coll} &\approx \frac{K p^2_{\rm coll}}{2m} + \frac{\langle p'^2 \rangle}{2m} \\ &= E^0_{\rm coll} + \frac{\langle p'^2 \rangle}{2m}. \end{aligned} \tag{A5}$$

Thus the apparent collective energy is larger than the true collective energy by a value of $\frac{\langle p'^2 \rangle}{2m}$. Rewriting Eq. (A5) in terms of the true collective excitation energy per nucleon, one gets

$$\begin{aligned} \frac{E^0_{\rm coll}}{K} &= \frac{E^a_{\rm coll}}{K} - \frac{1}{K}\frac{\langle p'^2 \rangle}{2m} \\ &= \frac{E^a_{\rm coll}}{K} - \varepsilon_{\rm corr}, \end{aligned} \tag{A6}$$

with

$$\varepsilon_{\rm corr} = \frac{1}{K}\frac{\langle p'^2 \rangle}{2m}. \tag{A7}$$

This correction to the collective excitation energy is due to the finite number of test particles. We note here that p'^2 is viewed in the frame of the true local velocity and is not known. In the following two sections, we describe two different methods to estimate $\langle p'^2 \rangle$.

1. Thomas-Fermi approximation

Since $\mathbf{p}'$ is evaluated in a frame moving with local current, one may estimate $\varepsilon_{\rm corr}$ in the local Thomas-Fermi approximation [125]. Using this assumption, Eq. (A7) becomes

$$\varepsilon_{\rm corr} = \frac{1}{K}\frac{\langle p'^2 \rangle}{2m} \approx \frac{1}{K}\frac{3}{5}\epsilon_F. \tag{A8}$$

Here the local Fermi energy ϵ_F is given by

$$\epsilon_F = \frac{p_F^2}{2m}, \tag{A9}$$

with

$$p_F = \hbar \left(\frac{3\pi^2 \rho}{2} \right)^{1/3}. \tag{A10}$$

In these expressions, we have assumed that the proton and neutron have the same local Fermi energy.

For a lattice cell of size 1 fm^{-3}, with local density of $\rho_0 = 0.17$ fm^{-3} and $N_{\rm test} = 80$, one would obtain $K \approx 14$, thus the correction to the collective energy would be $\varepsilon_{\rm corr} \approx 1.7$ MeV/nucleon. This is clearly a non-negligible correction. As we discussed in the main text, we have calculated the collective energy for a nucleus in its ground state. After correcting the local energy by a term given by Eq. (A8), one indeed obtains a zero collective energy.

2. Local momentum analysis

Another way of calculating $\langle p'^2 \rangle$ in Eq. (A7) is to try to determine it from the momentum distribution for $\mathbf{p}_i$, which is calculated as a function of time during the BUU simulations. For this purpose, we use the identity

$$\sum_{i \neq j} (\mathbf{p}_i - \mathbf{p}_j)^2 = \sum_{i \neq j} (\mathbf{p}_i{}' - \mathbf{p}_j{}')^2. \tag{A11}$$

Averaging over ensembles, the right-hand-side of this equation becomes

$$\begin{aligned} \left\langle \sum_{i \neq j} (\mathbf{p}_i{}' - \mathbf{p}_j{}')^2 \right\rangle &= 2K(K-1)\langle p'^2 \rangle \\ &\quad - 2 \left\langle \sum_{i \neq j} (\mathbf{p}_i{}' \cdot \mathbf{p}_j{}') \right\rangle. \end{aligned} \tag{A12}$$

The second term on the right-hand side of Eq. (A12) is of order $1/A$ times the first term and can be ignored in the limit of large A. Thus,

$$\left\langle \sum_{i \neq j} (\mathbf{p}_i{}' - \mathbf{p}_j{}')^2 \right\rangle \approx 2K(K-1)\langle p'^2 \rangle. \tag{A13}$$

Similarly, the left hand side of Eq. (A11) has the form

$$\begin{aligned} \left\langle \sum_{i \neq j} (\mathbf{p}_i - \mathbf{p}_j)^2 \right\rangle &= 2(K-1) \sum_{i=1}^{K} \langle p_i^2 \rangle \\ &\quad - 2 \left\langle \sum_{i \neq j} \mathbf{p}_i \cdot \mathbf{p}_j \right\rangle. \end{aligned} \tag{A14}$$

Using the identity

$$\left\langle \sum_{i \neq j} \mathbf{p}_i \cdot \mathbf{p}_j \right\rangle = \left\langle \left(\sum_{i=1}^{K} \mathbf{p}_i \right)^2 \right\rangle - \left\langle \sum_{i=1}^{K} p_i^2 \right\rangle, \tag{A15}$$

we can rewrite (A14) as

$$\left\langle \sum_{i \neq j} (\mathbf{p}_i - \mathbf{p}_j)^2 \right\rangle = 2K \left[\sum_{i=1}^{K} \langle p_i^2 \rangle - K \left\langle \left(\frac{\sum_{i=1}^{K} \mathbf{p}_i}{K} \right)^2 \right\rangle \right] = 2K \left\langle \sum_{i=1}^{K} \left[p_i^2 - \left(\frac{\sum_{i=1}^{K} \mathbf{p}_i}{K} \right)^2 \right] \right\rangle. \tag{A16}$$

Here the term

$$\frac{1}{2m}\left(\frac{\sum_{i=1}^{K}\mathbf{p}_i}{K}\right)^2$$

is the apparent collective energy. Equating Eqs. (A13) and (A16), one obtains

$$\varepsilon_{\rm corr}=\frac{1}{2m}\frac{1}{K(K-1)}\left\langle\sum_{i=1}^{K}\left[p_i^2-\left(\frac{\sum_{i=1}^{K}\mathbf{p}_i}{K}\right)^2\right]\right\rangle, \tag{A17}$$

which can be evaluated at each lattice point. This expression corrects for all spurious collective motion coming from either Fermi motion or thermal motion or both. This is the spurious collective energy correction used in this work and referred to in the main text.

[1] *Proceedings of the Symposium on Central Collisions and Fragmentation Processes* 1987, edited by C.K. Gelbke [Nucl. Phys. **A471**, 1c–451c (1987)].

[2] W. G. Lynch, Annu. Rev. Nucl. Sci. **37**, 493 (1987), and references contained therein.

[3] C. K. Gelbke and D. H. Boal, Prog. Part. Nucl. Phys. **19**, 33 (1987), and references contained therein.

[4] D. Guerreau, *Proceedings of the NATO Workshop on Nuclear Matter and Heavy Ion Collisions*, NATO ASI Series B: Physics, Vol. 205, (Plenum, New York, 1989), p. 187.

[5] E. Suraud, C. Gregoire, and B. Tamain, Prog. Part. Nucl. Phys. **23**, 357 (1989).

[6] L.G. Moretto, Phys. Lett. **40B**, 185 (1972).

[7] L. G. Moretto, Nucl. Phys. **A247**, 211 (1975).

[8] W. A. Friedman and W. G. Lynch, Phys. Rev. C **28**, 16 (1983).

[9] L. G. Sobotka, M. L. Padgett, G. J. Wozniak, G. Guarino, A. J. Pacheco, L. G. Moretto, Y. Chan, R. G. Stokstad, I. Tserruya, and S. Wald, Phys. Rev. Lett. **51**, 2187 (1983).

[10] L. G. Sobotka, M. A. McMahan, R. J. McDonald, C. Signarbieux, G. J. Wozniak, M. L. Padgett, J. H. Gu, Z. H. Liu, Z. Q. Yao, and L. G. Moretto, Phys. Rev. Lett. **53**, 2004 (1984).

[11] E. Plagnol, *et al.* Phys. Lett. B **221**, 11 (1989).

[12] C. B. Chitwood, D. J. Fields, C. K. Gelbke, W. G. Lynch, A. D. Panagiotou, M. B. Tsang, H. Utsunomiya, and W. A. Friedman, Phys. Lett. **131B**, 289 (1983).

[13] C. B. Chitwood, D. J. Fields, C. K. Gelbke, D. R. Klesch, W. G. Lynch, M. B. Tsang, T. C. Awes, R. L. Ferguson, F. E. Obenshain, F. Plasil, R. L. Robinson, and G. R. Young, Phys. Rev. C **34**, 858 (1986).

[14] M. B. Tsang, C. B. Chitwood, D. J. Fields, C. K. Gelbke, D. R. Klesch, W. G. Lynch, K. Kwiatkowski, and V. E. Viola, Jr., Phys. Rev. Lett. **52**, 1967 (1984).

[15] M. B. Tsang, R. M. Ronningen, G. Bertsch, Z. Chen, C. B. Chitwood, D. J. Fields, C. K. Gelbke, W. G. Lynch, T. Nayak, J. Pochodzalla, T. Shea, and W. Trautmann, Phys. Rev. Lett. **57**, 559 (1986).

[16] M. B. Tsang, Y. D. Kim, N. Carlin, Z. Chen, C. K. Gelbke, W. G. Gong, W. G. Lynch, T. Murakami, T. Nayak, R. M. Ronningen, H. M. Xu, F. Zhu, L. G. Sobotka, D. W. Stracener, D. G. Sarantites, Z. Majka, and V. Abenante, Phys. Rev. C **42**, R15 (1988).

[17] D. J. Fields, W. G. Lynch, C. B. Chitwood, C. K. Gelbke, M. B. Tsang, H. Utsunomiya, and J. Aichelin, Phys. Rev. C **30**, 1912 (1984).

[18] D. J. Fields, W. G. Lynch, T. K. Nayak, M. B. Tsang, C. B. Chitwood, C. K. Gelbke, R. Morse, J. Wilczynski, T. C. Awes, R. L. Ferguson, F. Plasil, F. E. Obenshain, and G. R. Young, Phys. Rev. C **34**, 536 (1986).

[19] J. Pochodzalla, C. B. Chitwood, D. J. Fields, C. K. Gelbke, W. G. Lynch, M. B. Tsang, D. H. Boal, and J. C. Shillcock, Phys. Lett. **174B**, 36 (1986).

[20] W. K. Wilson, W. Benenson, D. A. Cebra, J. Clayton, S. Howden, J. Karn, T. Li, C. A. Ogilvie, A. Vander Molen, G. D. Westfall, J. S. Winfield, B. Young, and A. Nadasen, Phys. Rev. C **41**, R1881 (1990).

[21] W. G. Gong, C. K. Gelbke, N. Carlin, R. T. de Souza, Y. D. Kim, W. G. Lynch, T. Murakami, G. Poggi, D. Sanderson, M. B. Tsang, H. M. Xu, D. E. Fields, K. Kwiatkowski, R. Planeta, V. E. Viola, Jr., S. J. Yennello, and S. Pratt, Phys. Lett. B **246**, 21 (1990).

[22] S. Leray, J. Phys. (Paris), Colloq. **47**, C4–275 (1986), and references therein.

[23] G. Auger, D. Jouan, E. Plagnol, F. Pougheon, F. Naulin, H. Doubre, and C. Grégoire, Z. Phys. A **321**, 243 (1985).

[24] G. Auger, E. Plagnol, D. Jouan, C. Guet, D. Heuer, M. Maurel, H. Nifenecker, C. Ristori, F. Schussler, H. Doubre, and C. Grégoire, Phys. Lett. **169B**, 161 (1986).

[25] D. Jacquet, E. Duek, J. M. Alexander, B. Borderie, J. Galin, D. Gardes, D. Guerreau, M. Lefort, F. Monnet, M. F. Rivet, and X. Tarrago, Phys. Rev. Lett. **53**, 2226 (1984).

[26] M. Conjeaud, S. Harar, M. Mostefai, E. C. Pollacco, C. Volant, Y. Cassagnou, R. Dayras, R. Legrain, H. Oeschler, and F. Saint-Laurent, Phys. Lett. **159B**, 244 (1985).

[27] C. Volant, M. Conjeaud, S. Harar, M. Mostefai, E. C. Pollacco, Y. Cassagnou, R. Dayras, R. Legrain, G. Klotz-Engmann, and H. Oeschler, Phys. Lett. B **195**, 22 (1987).

[28] A. Fahli, J. P. Coffin, G. Guillaume, B. Heusch, F. Jundt, F. Rami, P. Wagner, P. Fintz, A.J. Cole, S. Kox, and Y. Schutz, Phys. Rev. C **34**, 161 (1986).

[29] H. Nifenecker, J. Blachot, J. Crancon, A. Gizon, and A. Lleres, Nucl. Phys. **A447**, 533c (1985).

[30] B. Borderie and M. F. Rivet, Z. Phys. A **321**, 703 (1985).

[31] K. A. Griffioen, R. J. Meijer, P. F. Box, P. Decowski, G. J. Van Nieuwenhuizen, R. Kamermans, H. W. Wilschut, A. Giorni, C. Morand, A. Demeyer, and D. Guinet, Phys. Lett. B **237**, 24 (1990).

[32] P. Decowski *et al.*, in Proceedings of the XXVIII International Winter Meeting on Nuclear Physics, Bormio, Italy, 1990 (unpublished).

[33] J. Galin, Nucl. Phys. **A488**, 297c (1988).

[34] D. Jacquet, J. Galon, B. Borderie, D. Gardes, D. Guer-

reau, M. Lefort, F. Monnet, M. F. Rivet, X. Tarrago, E. Duek, and J. M. Alexander, Phys. Rev. C **32**, 1594 (1985).

[35] J. B. Natowitz, M. Gonin, K. Hagel, R. Wada, S. Shlomo, X. Bin, M. Gui, Y. Lou, D. Utley, T. Botting, R. K. Choudhury, L. Cooke, B. Hurst, D. O'Kelly, R. P. Schmitt, W. Turmel, H. Utsonomiya, G. Nebbia, D. Fabris, J. A. Ruiz, G. Nardelli, M. Poggi, R. Zanon, G. Viesti, R. H. Burch, F. Gramegna, G. Prete, D. Drain, B. Chambon, B. Cheynis, D. Guinet, X. C. Hu, A. Demeyer, C. Pasteur, A. Giorni, A. Lleres, P. Stassi, B. Viano, A. Menchaca Rocha, M. E. Brandan, and P. Gonthier, Nucl. Phys. **A538**, 263c (1992).

[36] D. Fabris *et al.*, Nucl. Phys. **A471**, 351c (1987); Phys. Lett. B **196**, 429 (1987).

[37] M. Gonin, J. P. Coffin, G. Guillaume, F. Jundt, P. Wagner, P. Fintz, B. Heusch, A. Malki, A. Fahli, S. Kox, F. Merchez, and J. Mistretta, Phys. Rev. C **38**, 135 (1988).

[38] K. Hagel, D. Fabris, P. Gonthier, H. Ho, Y. Lou, Z, Majka, G. Mouchaty, M. N. Namboodiri, J. B. Natowitz, G. Nebbia, R. P. Schitt, G. Viesti, R. Wada,and B. Wilkins, Nucl. Phys. **A486**, 429 (1988).

[39] M. Gonin, L. Cooke, K. Hagel, Y. Lou, J. B. Natowitz, R. P. Schitt, B. Srivastava, W. Turmel, H. Utsunomiya, R. Wada, B. Fornal, G. Nardelli, G. Nebbia, G. Viesti, R. Zanon, G. Prete, P. Gonthier, and B. Wilkins, Phys. Lett. B **217**, 406 (1989).

[40] M. Gonin, L. Cooke, K. Hagel, Y. Lou, J. B. Natowitz, R. P. Schitt, S. Shlomo, B. Srivastava, W. Turmel, H. Utsunomiya, R. Wada, G. Nardelli, G. Nebbia, G. Viesti, R. Zanon, B. Fornal, G. Prete, K. Niita, S. Hannuschke, P. Gonthier, and B. Wilkins, Phys. Rev. C **42**, 2125 (1990).

[41] S. Song, M. F. Rivet, R. Bimbot, B. Borderie, I. Forest, J. Galin, D. Gardes, B. Gatty, M. Lefort, H. Oeschler, B. Tamain, and X. Tarrago, Phys. Lett. **130B**, 14 (1983).

[42] D. Hilscher, H. Rossner, A. Gamp, U. Jahnke, B. Cheynis, B. Chambon, D. Drain, C. Paster, A. Giorni, C. Morand, A. Dauchy, P. Stassi, and G. Petitt, Phys. Rev. C **36**, 208 (1987).

[43] R. Wada, D. Fabris, K. Hagel, G. Nebbia, Y. Lou, M. Gonin, J. B. Natowitz, R. Billerey, B. Cheynis, A. Demeyer, D. Drain, D. Guinet, C. Pastor, L. Vagneron, K. Zaid, J. Alarja, A. Giorni, D. Heuer, C. Morand, B. Viano, C. Mazur, C. Ngô, S. Leray, R. Lucas, M. Ribrag, and E. Tomasi, Phys. Rev. C **39**, 497 (1989).

[44] D. X. Jiang, H. Doubre, J. Galin, D. Guerreau, E. Piasecki, J. Pouthas, A. Sokolov, B. Cramer, G. Ingold, U. Jahnke, E. Schwinn, J. L. Charvet, J. Frehaut, B. Lott, C. Magnago, M. Morjean, Y. Patin, Y. Pranal, J. L. Uzureau, B. Gatty, and D. Jacquet, Nucl. Phys. **A503**, 560 (1989).

[45] W. Bohne, H. Morgenstern, K. Grabisch, T. Nakagawa, and S. Proschitzki, Phys. Rev. C **41**, R5 (1990).

[46] A. Chbihi, L. G. Sobotka, N. G. Nicolis, D. G. Sarantites, D. W. Stracener, Z. Majka, D. C. Hersley, J. R. Beene, M. L. Halbert, Phys. Rev. C **43**, 666 (1991).

[47] D. J. Morrissey, W. Benenson, E. Kashy, B. Sherrill, A. D. Panagiotou, R. A. Blue, R. M. Ronningen, J. van der Plicht, and H. Utsunomiya, Phys. Lett. **148B**, 423 (1984).

[48] D. J. Morrissey, W. Benenson, E. Kashy, C. Bloch, M. Lowe, R. A. Blue, R. M. Ronningen, B. Sherrill, H. Utsunomiya, and I. Kelson, Phys. Rev. C **32**, 877 (1985).

[49] D. J. Morrissey, C. Bloch, W. Benenson, E. Kashy, R. A. Blue, R. M. Ronningen, and R. Aryaeinejad, Phys. Rev. **C34**, 761 (1986).

[50] H. M. Xu, D. J. Fields, W. G. Lynch, M. B. Tsang, C. K. Gelbke, M. R. Maier, D. J. Morrissey, J. Pochodzalla, D. G. Sarantites, L. G. Sobotka, M. L. Halbert, D. C. Hensley, D. Hahn, and H. Stocker, Phys. Lett. **182B**, 155 (1986).

[51] H. M. Xu, W. G. Lynch, C. K. Gelbke, M. B. Tsang, D. J. Fields, M. R. Maier, D. J. Morrissey, T. K. Nayak, J. Pochodzalla, D. G. Sarantites, L. G. Sobotka, M. L. Halbert, D. C. Hensley, Phys. Rev. C **40**, 186 (1989).

[52] J. Gomez del Campo, J. L. Charvet, A. D'Onofrio, R. L. Auble, J. R. Beene, M. L. Halbert, and H. J. Kim, Phys. Rev. Lett. **61**, 290 (1988).

[53] J. Gomez del Campo, R. L. Auble, J. R. Beene, M. L. Halbert, H. J. Kim, A. D'Onofrio, and J. L. Charvet, Phys. Rev. C **43**, 2689 (1991).

[54] Jeong Ho Lee, W. Benenson, and D. J. Morrissey, Phys. Rev. C **41**, 1562 (1990).

[55] J. Pochodzalla, W. A. Friedman, C. K. Gelbke, W. G. Lynch, M. Maier, D. Ardouin, H. Delagrange, H. Doubre, C. Gregoire, A. Kyanowski, W. Mittig, A. Peghaire, J. Peter, F. Saint-Laurent, Y. P. Viyogi, B. Zwieglinski, G. Bizard, F. Lefebvres, B. Tamain, J. Quebert, Phys. Lett. **161B**, 275 (1985).

[56] J. Pochodzalla, W. A. Friedman, C. K. Gelbke, W. G. Lynch, M. Maier, D. Ardouin, H. Delagrange, H. Doubre, C. Gregoire, A. Kyanowski, W. Mittig, A. Peghaire, J. Peter, F. Saint-Laurent, Y. P. Viyogi, B. Zwieglinski, G. Bizard, F. Lefebvres, B. Tamain, and J. Quebert, Phys. Rev. Lett. **55**, 177 (1985).

[57] J. Pochodzalla, C. K. Gelbke, W. G. Lynch, M. Maier, D. Ardouin, H. Delagrange, H. Doubre, C. Gregoire, A. Kyanowski, W. Mittig, A. Peghaire, J. Peter, F. Saint-Laurent, B. Zwieglinski, G. Bizard, F. Lefebvres, B. Tamain, J. Quebert, Y. P. Viyogi, W. A. Friedman, and D. H. Boal, Phys. Rev. C **35**, 1695 (1987).

[58] Z. Chen, C. K. Gelbke, J. Pochodzalla, C. B. Chitwood, D. J. Fields, W. G. Lynch, and M. B. Tsang, Phys. Lett. B **184**, 280 (1987).

[59] Z. Chen, C. K. Gelbke, J. Pochodzalla, C.B. Chitwood, D.J. Fields, W. G. Gong, W. G. Lynch, and M. B. Tsang, Nucl. Phys. **A473**, 564 (1987).

[60] Z. Chen, C. K. Gelbke, W. G. Gong, Y. D. Kim, W. G. Lynch, M. R. Maier, J. Pochodzalla, M. B. Tsang, F. Saint-Laurent, D. Ardouin, H. Delagrange, H. Doubre, J. Kasagi, A. Kyanowski, A. Peghaire, J. Peter, E. Rosato, G. Bizard, F. Lefebvres, B. Tamain, J. Quebert, and Y. P. Viyogi, Phys. Rev. C **36**, 2297 (1987).

[61] Z. Chen, C. K. Gelbke, W. G. Gong, Y. D. Kim, W. G. Lynch, M. R. Maier, J. Pochodzalla, M. B. Tsang, F. Saint-Laurent, D. Ardouin, H. Delagrange, H. Doubre, J. Kasagi, A. Kyanowski, A. Peghaire, J. Peter, E. Rosato, G. Bizard, F. Lefebvres, B. Tamain, J. Quebert, and Y. P. Viyogi, Phys. Lett. B **199**, 171 (1987).

[62] F. Saint-Laurent, A. Kyanowski, D. Ardouin, H. Delagrange, H. Doubre, C. Gregoire, W. Mittig, A. Peghaire, J. Peter, G. Bizard, F. Lefebvres, B. Tamain, J. Quebert, Y. P. Viyogi, J. Pochodzalla, C. K. Gelbke, W. Lynch, and M. Maier, Phys. Lett. B **202**, 190 (1988).

[63] D. Fox, D. A. Cebra, J. Karn, C. Parks, A. Pradhan, A. Vander Molen, J. van der Plicht, G. D. Westfall, W. K. Wilson, and R. S. Tickle, Phys. Rev. C **38**, 146 (1988).

[64] T. K. Nayak, T. Murakami, W. G. Lynch, K. Swartz, D. J. Fields, C. K. Gelbke, Y. D. Kim, J. Pochodzalla, M. B. Tsang, H. M. Xu, F. Zhu, and K. Kwiatkowski, Phys. Rev. Lett. **62**, 1021 (1989).
[65] T. K. Nayak, T. Murakami, W. G. Lynch, K. Swartz, D. J. Fields, C. K. Gelbke, Y. D. Kim, J. Pochodzalla, M. B. Tsang, H. M. Xu, F. Zhu, and K. Kwiatkowski, Phys. Rev. **C 45**, 132 (1992).
[66] F. Zhu, W. G. Lynch, D. R. Bowman, R. T. de Souza, C. K. Gelbke, Y. D. Kim, L. Phair, M. B. Tsang, C. Williams, H. M. Xu, and J. Dinius, Phys. Lett. B **282**, 299 (1992).
[67] G. J. Kunde, J. Pochodzalla, J. Aichelin, E. Berdermann, B. Berthier, C. Cerruti, C. K. Gelbke, J. Hubele, P. Kreutz, S. Leray, R. Lucas, U. Lynen, U. Milkau, W. F. J. Müller, C. Ngõ, C. H. Pinkenburg, G. Raciti, H. Sann, and W. Trautmann, Phys. Lett. B **272**, 202 (1991).
[68] C. Bloch, W. Benenson, E. Kashy, D. J. Morrissey, R. A. Blue, R. M. Ronningen, and H. Utsunomiya, Phys. Rev. C **34**, 850 (1986).
[69] C. Bloch, W. Benenson, A. I. Galonsky, E. Kashy, J. Heltsley, L. Heilbronn, M. Lowe, B. Remington, D. J. Morrissey, and J. Kasagi, Phys. Rev. C **36**, 203 (1987).
[70] A. Galonsky, G. Caskey, L. Hilbronn, B. Remington, H. Schelin, F. Deák, A. Kiss, Z. Seres, and J. Kasagi, Phys. Lett. B **197**, 511 (1987).
[71] F. Deák, A. Kiss, Z. Seres, A. Galonsky, C. K. Gelbke, L. Heilbronn, W. Lynch, T. Murakami, H. Schelin, M. B. Tsang, B. A. Remington, and J. Kasagi, Phys. Rev. C **39**, 733 (1989).
[72] L. Heilbronn, A. Galonsky, C. K. Gelbke, W. G. Lynch, T. Murakami, D. Sackett, H. Schelin, M. B. Tsang, F. Deák, A. Kiss, Z. Seres, J. Kasagi, and B. A. Remington, Phys. Rev. C **43**, 2318 (1991).
[73] C. B. Chitwood, C. K. Gelbke, J. Pochodzalla, Z. Chen, D. J. Fields, W. G. Lynch, R. Morse, M. B. Tsang, D. H. Boal, and J. C. Shillcock, Phys. Lett. **172B**, 27 (1986).
[74] W. A. Friedman, Phys. Rev. C **42**, 667 (1990).
[75] W. A. Friedman, Phys. Rev. Lett. **60**, 2125 (1988).
[76] S. E. Koonin and J. Randrup, Nucl. Phys. **A474**, 173 (1987).
[77] J. Randrup, Nucl. Phys. **A495**, 245c (1989).
[78] G. Bertsch and P. J. Siemens, Phys. Lett. **126B**, 9 (1983).
[79] H. Sagawa and G. F. Bertsch, Phys. Lett. **155B**, 11 (1985).
[80] J. E. Finn, S. Agarwal, A. Bujak, J. Chuang, L. J. Gutay, A. S. Hirsch, R. W. Minich, N. T. Porile, R. P. Scharenberg, B. C. Stringfellow, and F. Turkot, Phys. Rev. Lett. **49**, 1321 (1982).
[81] D. J. Fields, C. K. Gelbke, W. G. Lynch, and J. Pochodzalla, Phys. Lett. B **187**, 257 (1987).
[82] S. Levit and P. Bonche, Nucl. Phys. **A437**, 426 (1984).
[83] J. Besprosvany and S. Levit, Phys. Lett. B **217**, 1 (1989).
[84] D. Bandyopadhyay, S. K. Samaddar, R. Saha, and J. N. De, Nucl. Phys. **A539**, 370 (1992).
[85] S. Ban-Hao and D. H. E. Gross, Nucl. Phys. **A437**, 643 (1985).
[86] D. H. E. Gross, Phys. Lett. B **203**, 26 (1988).
[87] D. H. E. Gross, L. Satpathy, Mang Ta-Chung, and M. Satpathy, Z. Phys. A **309**, 41 (1982).
[88] D. H. E. Gross, Zhang Xiao-ze, and Xu Shu-yan, Phys. Rev. Lett. **56**, 1544 (1986).
[89] Zhang Xiao-ze, D. H. E. Gross, and S. Y. Xu and Y. M. Zheng, Nucl. Phys. **A461**, 668 (1987).
[90] J. P. Bondorf, S. I. A. Garpman, and J. Zimanyi, Nucl. Phys. **A296**, 320 (1978).
[91] J. Bondorf *et al.*, Phys. Lett. **162B**, 30 (1985); Nucl. Phys. **A443**, 321 (1985).
[92] Z. Chen and C. K. Gelbke, Phys. Rev. C **38**, 2630 (1988).
[93] D. Hahn and H. Stocker, Phys. Rev. C **35**, 1311 (1987).
[94] J. A. Lopez and P. J. Siemens, Nucl. Phys. **A431**, 728 (1984).
[95] A. Z. Mekjian, Phys. Rev. Lett. **18**, 2125 (1990).
[96] H. W. Barz, H. Schulz, and G. F. Bertsch, Phys. Lett. B **217**, 397 (1989).
[97] S. Shlomo and J. B. Natowitz, Phys. Lett. B **252**, 187 (1990); Phys. Rev. C **44**, 2878 (1991).
[98] T. J. Schlagel and V. R. Pandharipande, Phys. Rev. C **36**, 162 (1987).
[99] R. J. Lenk and V. R. Pandharipande, Phys. Rev. C **34**, 177 (1986).
[100] K. Sneppen and L. Vinet, Nucl. Phys. **A480**, 342 (1988).
[101] D. H. Boal and A. L. Goodman, Phys. Rev. C **33**, 1690 (1986).
[102] D. H. Boal and J. N. Glosli, Phys. Rev. C **37**, 91 (1988); **38**, 1870 (1988).
[103] D. H. Boal, J. N. Glosli, and C. Wicentowich, Phys. Rev. Lett. **62**, 737 (1989); Phys. Rev. C **40**, 601 (1989).
[104] B. Remaud, C. Grégoire, F. Sébille, and P. Schuck, Nucl. Phys. **A488**, 423c (1988).
[105] B. Remaud, C. Grégoire, F. Sébille, and L. Vinet, Phys. Lett. **180B**, 198 (1986).
[106] E. Suraud, M. Pi, P. Schuck, B. Remaud, F. Sébille, C. Grégoire and F. Saint-Laurent, Phys. Lett. B **229**, 359 (1989).
[107] E. Suraud, Proceeding of the XXVIII International Winter Meeting on Nuclear Physics, Bornio, Italy, 1990 (unpublished).
[108] E. Suraud, D. Cussol, Ch. Grégoire, D. Boilley, M. Pi, P, Schuck, B. Remaudm, and F. Sébille, Nucl. Phys. **A495**, 73c (1989).
[109] S. Bhattacharya, J. N. De, K. Krishan, and S. K. Samaddar, Phys. Rev. Lett. **62**, 2589 (1989).
[110] H. M. Xu, W. G. Lynch, P. Danielewicz, and G. F. Bertsch, Phys. Rev. Lett. **65**, 843 (1990).
[111] H. M. Xu, W. G. Lynch, P. Danielewicz, and G. F. Bertsch, Phys. Lett. B **261**, 240 (1991).
[112] H. M. Xu, Ph.D. dissertation, Michigan State University, East Lansing, Michigan, 1991 (unpublished).
[113] H. M. Xu, Phys. Rev. Lett. **67**, 2769 (1992); Phys. Rev. C **46**, R389 (1992).
[114] H. M. Xu, P. Danielewicz, and W. G. Lynch, Phys. Lett. B **299**, 199 (1993); H. M. Xu, Nucl. Phys. **A568**, 365 (1994).
[115] H. M. Xu, Phys. Rev. C **46**, R2144 (1992); H. M. Xu, J. B. Natowitz, C. A. Gargliardi, R. E. Tribble, C. Y. Wong, and W. G. Lynch, Phys. Rev. C **48**, 933 (1993).
[116] G. F. Bertsch and S. Das Gupta, Phys. Rep. **160**, 189 (1988), and references contained therein.
[117] C. Y. Wong, Phys. Rev. C **25**, 1460 (1982).
[118] G.F. Bertsch, H. Kruse, and S. Das Gupta, Phys. Rev. C **29**, 673 (1984).
[119] J. Aichelin and G. Bertsch, Phys. Rev. C **331**, 1730

(1985).
[120] H. Kruse, B. V. Jacak, and H. Stöcker, Phys. Rev. Lett. **54**, 289 (1985).
[121] J. J. Molitoris and H. Stöcker, Phys. Rev. C **32**, 346(1985); Phys. Lett. **162B**, 47(1985).
[122] R. J. Lenk and V. R. Pandharipande, Phys. Rev. C **39**, 2242 (1989).
[123] Amos Shalit and Herman Feshbach, *Nuclear Structure*, Theoretical Nuclear Physics Volume I (Wiley, New York, 1974), p. 8.
[124] W. Cassing, Z. Phys. A **327**, 447 (1987).
[125] A. S. Goldhaber, Phys. Lett. **53B**, 306 (1974).